Fracturing Material Models Based on Micromechanical Concepts: Recent Advances

Z.P. Bažant
McCormick School of Engineering and Applied Science, 2145 Sheridan Road, Northwestern University, Evanston, Illinois 60201, U.S.A.

F.C. Caner
Department of Geotechnical Engineering, Technical University of Catalunya, Barcelona, Spain

L. Cedolin, G. Cusatis & G. Di Luzio
Department of Structural Engineering, Politecnico di Milano, Milano, Italy

ABSTRACT: The paper summarizes three recent advances in the modeling of inelastic behavior and fracturing of concrete, achieved at Northwestern University and Politecnico di Milano. First, improvements of microplane model M4 which allow a more realistic simulation of frictional shear and of lateral strains in tensile fracturing are presented. Second, development of microplane model M5 which can capture the transition from distributed cracking damage to complete cohesive fracture is described and its novel concept—a combination of kinematic and static constraints— is discussed. Third, a new lattice type model for concrete, which can simulate (with the same material parameters) tensile fracturing, complete cohesive fracture, compression-shear behavior with softening at zero or mild confinement, and response at confined compression at which there is only hardening (i.e., no peal and no postpeak softening), is outlined.

Keywords: microplane model, lattice models, damage, fracture, concrete, microstructure simulation.

1 IMPROVEMENTS OF MICROPLANE MODEL M4

The microplane model evolved from the slip theory of plasticity, which was developed by Batdorf & Budianski (1949) on the basis of the original idea of G.I. Taylor (1938). This theory has been extensively applied to plasticity of metals and its improvements continue until today (e.g., Brocca & Bažant 2000, Bronkhorst et al. 1992, Butler & McDowell 1998). In the early 1980s, this idea was modified and extended at Northwestern University to quasi-brittle materials with strain-softening. To achieve a stable and unique solution for a softening material, the static constraint of the slip theory of plasticity has been replaced (Bažant 1984) by the kinematic constraint, in which the microplane strain components are calculated as the projections of the macroscopic strain tensor. The microplane model trades extensive computations (which are no longer an obstacle) for conceptual simplicity of a three-dimensional formulation and versatile data fitting capability (Bažant & Prat 1988, Bažant & Ožbolt 1990, Bažant et al. 1996, Bažant et al. 2000, Caner & Bažant 2000). To control the value of Poisson's ratio and model compressive failures, a split of normal microplane components into their volumetric and deviatoric parts was introduced (in model M2; Bažant & Prat 1988). However, the volumetric-deviatoric split was made thermodynamically consistent only in model M4.

The volumetric-deviatoric split introduced in model M2 caused deficient simulation of the tensile behavior. To mitigate this deficiency, model M3 introduced softening strain-dependent yield limits called stress-strain boundaries imposed separately on the volumetric and deviatoric stress components on each microplane. In model M4, the deficient tensile behavior was almost cured by adding a tensile boundary for the total normal stress, which ensured the tensile stress to reduce to zero at sufficiently large tensile strain. But the cure was incomplete—the lateral strains at very large uniaxial tensile strains were unrealistic and hard to control, and the lateral strains did not reduce exactly to zero (Fig. 1b).

To eliminate the problem with lateral strains in tension, Di Luzio et al. (2003) proposed an alternative approach in which the tensile volumetric boundary is removed (the boundary on total tensile strain being retained) and a smooth *transition function* φ depending on the maximum principal strain σ_I and the volumetric strain ε_v is introduced in order to gradually remove the

volumetric-deviatoric split on approach to very large tensile strains. Thus, the normal stress on the microplanes is, according to di Luzio et al. (2003), calculated through the following formula:

$$\sigma_N = \varphi \sigma_N^{\text{no split}} + (1-\varphi)\sigma_N^{\text{split}} \quad (1)$$

where $\sigma_N^{\text{no split}}$ and σ_N^{split} are given by

$$\sigma_N^{\text{no split}} = \sigma_N^{\text{no split, pre}} + E_N \Delta\varepsilon_N \le \sigma_N^b$$
$$\sigma_N^{\text{split}} = \sigma_D + \sigma_V \le \sigma_N^b \quad (2)$$

The transition function φ is 0 unless the tensile postpeak regime is reached. After that, φ gradually increases to 1, thus effecting a transition to the formulation with no split of the normal components for all the microplanes (various definitions of φ for arbitrary loading paths are still being explored but a linear variation of φ as a function of ε_N from the strain at the peak of ε_N to a double or triple of that strain appears to work).

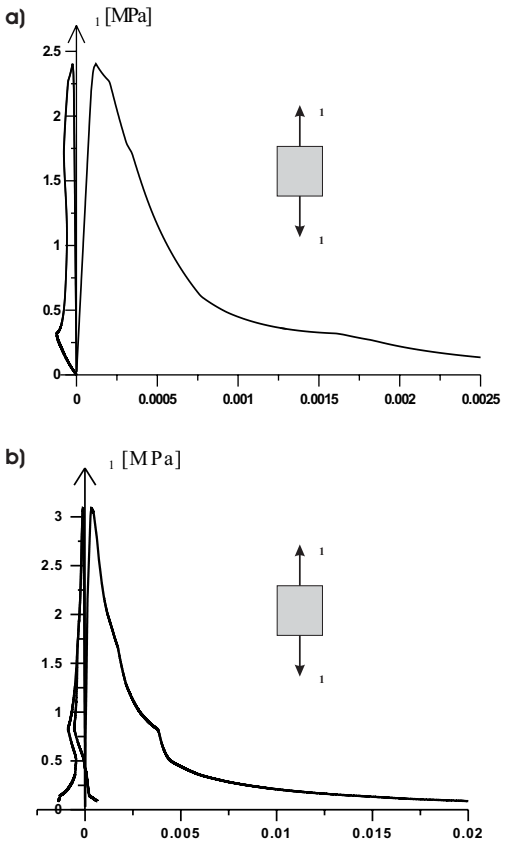

Figure 1. Stress-strain curves for uniaxial tension: a) using the transition function; b) original M4 formulation.

Calculating the normal stress as indicated in Equation 1, one obtains for uniaxial tension the macroscopic stress-strain curves plotted in Figure 1a, which show that the deficient (non-zero) far-out tail of the tensile response has been cured.

Another improvement has been made in the frictional boundary on the microplanes. model M4 first calculates the shear stress at the boundary as $\sigma^b_T = F_T(\sigma_N)$ and the elastic shear stresses as $\sigma^e_L = \sigma^{pre}_L + E_T \Delta\varepsilon_L$ and $\sigma^e_M = \sigma^{pre}_M + E_T \Delta\varepsilon_M$. For calculating the shear stress, there are two alternatives: *Alt. I* — (used originally in M4): Calculate the shear stresses in ***l*** and ***m*** directions imposing independently the shear boundary on the two components as $\sigma_L = \text{sign}(\sigma^e_L)$ min $(|\sigma^b_T|, |\sigma^e_L|)$ and $\sigma_M = \text{sign}(\sigma^e_M)$ min $(|\sigma^b_T|, |\sigma^e_M|)$.

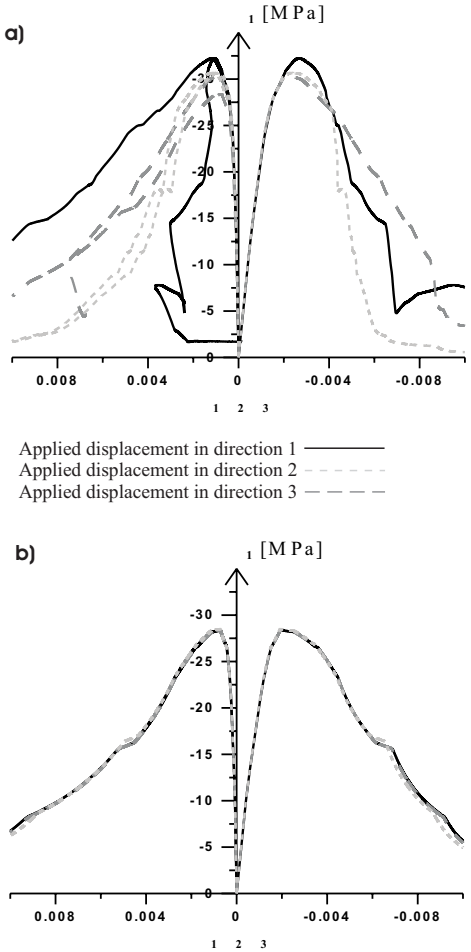

Figure 2. Stress-strain curves for uniaxial compression with different direction of applied displacement: a) using *Alt-I*; b) using *Alt-II*.

Alt. II — Calculate the resultant of the elastic shear stresses as $\sigma^{eR}_T=[(\sigma^e_L)^2+(\sigma^e_M)^2]^{1/2}$; determine the unit vector in the resultant direction, $\boldsymbol{R}= (\sigma^e_L, \sigma^e_M)/\sigma^{eR}_T$; impose the shear boundary on the resultant of the elastic shear stresses, $\sigma^R_T = \min(\sigma^b_T, \sigma^{eR}_T)$; and compute the shear stresses as $(\sigma_L, \sigma_M)=\sigma^R_T$ **R**. Although both alternatives were considered in M4 from the outset, Di Luzio et al. (2003) was first to demonstrate that *Alt. I* leads to appreciably different responses for normal strains imposed in different directions. Figure 2a shows the stress-strain curves for uniaxial compression simulations for strains imposed in three different directions; note that the model prediction varies significantly with the direction of the applied strain. *Alt. II* removes this drawback; see Figure 2b, where the response curves for the same applied strains as in Figure 2a become essentially coincident.

2 MICROPLANE MODEL M5 WITH TRANSITION TO COHESIVE FRACTURE

A generalization of microplane mode M4, labeled M5 (Bažant & Caner 2002), has recently been developed to simulate transition to complete fracture in the sense of the cohesive crack model (introduced to conrete under the name fictitious crack model by Hillerborg et al. 1976). This new model achieves a more realistic representation of progressive tensile cracking or cohesive fracture. It avoid stress locking which, in M4, prevented the stress from being reduced all the way to zero at very large tensile strains. Furthermore, like the improvement discussed in the preceding section, model M5 eliminates the spurious excessive lateral contraction or expansion which was exhibited by the original model M4 at very large postpeak tensile strains.

The improvement is achieved by a series coupling of two microplane systems, one constrained kinematically (model M4) and the other statically (Fig. 3). The latter simulates exclusively tensile cracking and fracture, while the former simulates all the nonlinear triaxial behavior in pure compression and compression with shear. It may be noted that the coupling bears some analogy with the finite element model of Camacho & Ortiz (1996), in which a cohesive crack model is inserted into each interface between two adjacent finite elements characterized by elastic or hardening elasto-plastic constitutive relations.

The coupling of two microplane systems is made possible by developing a new iterative algorithm which avoids solving the implicit nonlinear equations that relate the two microplane systems. A special characteristic of this algorithm is that, in each loading step, the softening cohesive fracture properties of the statically constrained microplanes are used as the predictor and the hardening or unloading properties of the kinematically constrained microplanes are used as the corrector that returns the current state point to the stress-strain boundaries (softening yield limits). The roles of predictor and corrector are interchanged compared to the classical iterative return mapping algorithms for hardening elasto-plastic behavior.

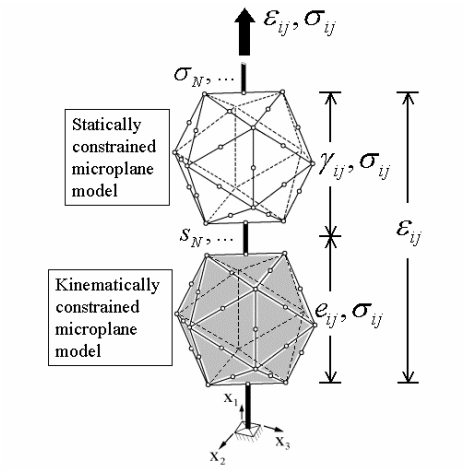

Figure 3: Microplane model M5, characterized by coupling of kinematically and statically constrained microplane systems for hardening and softening responses

It has been proven that the new iterative algorithm converges in the form of a geometric progression, and the conditions of convergence have been derived (Bažant & Caner 2002).

Except for a few minor differences, the constitutive properties on the kinematically constrained microplanes are the same as in the previous model M4. The far post-peak tensile softening excepted, the response is the same.

The softening cohesive fracture properties are related to the fracture energy and effective crack spacing. The post-peak softening slope on the microplanes can be adjusted in the sense of the crack band model, to ensure the correct energy dissipation of localized fracture when the finite element size is varied. The constitutive properties that differ from the original model M4 are shown to allow good representation of test data for tensile softening of concrete and of the shear-compression failure envelope of concrete.

A thermodynamic potential for the coupling of statically and kinematically constrained microplane systems has also been formulated. In the case of isothermal conditions, it represents a combination of the Helmholtz and Gibbs free energy densities (Bažant & Caner 2002).

3 CONFINEMENT-SHEAR LATTICE MODEL

3.1 *Brief review of the model*

The *Confinement-Shear Lattice model* (*CSL* model) is a model in which the concrete mesostructure is simulated by a lattice connecting particles that represent the aggregate pieces. The particle center coordinates (lattice nodes) are generated randomly but such a way that the given granulometric distribution of the aggregate sizes is followed. Only aggregate sizes larger than a certain limit are considered in order to avoid excessive computational time. The inter-particle links (struts) simulate the contact layers of mortar between two aggregate pieces. These links are defined according to a Delaunay triangulation of the center points of the aggregates.

The contact layer can transmit both the normal and shear stresses, which are assumed to be functions of normal and shear strains which, in turn, are defined, incrementally, as $d\varepsilon_N=(du_2-du_1)/l$, $d\varepsilon_M=(dv_2-dv_1-l_2 d\theta_2-l_1 d\theta_1)/l$, $d\varepsilon_L=(dw_2-dw_1+l_2 d\phi_2-l_1 d\phi_1)/l$. Here u_1, u_2 are the displacements of the two connected aggregate in the direction of the line connecting their centers, v_1, v_2, w_1 and w_2 are the transversal displacements and θ_1, θ_2, ϕ_1 and ϕ_2 are the spatial rotations of the aggregates. The lengths l_1 and l_2 define the position of the contact point. All the strain components are assumed uniformly smeared over length l of the connection. The stress-strain relations are given as

$$\sigma_N = \frac{\sigma}{\varepsilon}\varepsilon_N;\quad \sigma_M = \alpha\frac{\sigma}{\varepsilon}\varepsilon_M;\quad \sigma_L = \alpha\frac{\sigma}{\varepsilon}\varepsilon_L \qquad (3)$$

in which σ (*effective stress*) is assumed to be a function of $\varepsilon=(\varepsilon_N^2+\alpha\varepsilon_T^2)^{1/2}$ (*effective strain*) and $\omega=\arctan[\varepsilon_N/(\alpha^{1/2}\varepsilon_T)]$ (*coupling strain*) where $\varepsilon_T=(\varepsilon_M^2+\varepsilon_L^2)^{1/2}$ is the *total shear strain*; and α is a constant material parameter which represents the ratio between shear and normal stiffnesses of the connecting strut.

The elastic behavior is modeled by the incremental relation $d\sigma=Ed\varepsilon$. The nonlinear behavior is simulated by using the concept of stress-strain boundary (strain-dependent yield limit) which is imposed by the inequality $0\le\sigma\le\sigma_b$ where

$$\sigma_b = \sigma_0(\omega)\exp\left(K(\omega)\frac{\langle\varepsilon-\varepsilon_0(\omega)\rangle}{\sigma_0(\omega)}\right) \qquad (4)$$

Here $\sigma_0(\omega)$ is the effective strength, $\varepsilon_0(\omega)=\sigma_0(\omega)/E$ is the elastic strain limit, and $K(\omega)$ governs the stress evolution in the non linear range. $K(\omega)$ is negative (softening behavior) for tension, shear with tension, and shear with low compression, but it is positive (hardening behavior) for compression and shear with high compression. For tension dominated stress states, the post-peak behavior at the meso-level is also assumed to be sensitive to the confining stress transversal to the connecting strut between particles. This feature endows the present model with the capability of simulating not only the tensile softening and failure but also (in contrast to previous models) the compression softening and failure in unconfined tests as well as the lack of softening and of peak stress under confined compression and under pure hydrostatic pressure. The confinement effect on the connecting lattice struts reflects the effect of mortar whose tiny aggregate particles are too numerous for being included as lattice nodes. A detailed description and validation of the *CSL* model can be found in Cusatis et al. (2003a, b).

3.2 *New improvements*

Delaunay triangulation in three dimensions yields a system of tetrahedral whose edges are the lattice struts. A cross-sectional area needs to be assigned to each connecting strut such that the volume of all struts be equal to the volume of the solid filled by all the tetrahedra. In the original version of the model (Cusatis et al. 2003a, b), this goal was achieved as follows: 1) the volume of each tetrahedron was subdivided on its edges (each representing a connection between two adjacent aggregates) proportionally to their lengths, 2) the total volume of each strut was obtained by summing up the contributions of all adjacent tetrahedral, and 3) the effective cross-sectional area of the strut was determined by dividing the total volume of the strut by its length. The cross-section area and volume thus assigned to each connection is, of course, only approximate and its shape is implicitly considered as a cylinder. In recent computations, it has been noticed that the cross-section area, simulating the mesolevel crack surface area, tended to be underestimated, which, in turn, caused that the constitutive law assigned to each contact area at the mesolevel was not quite realistic.

A more realistic estimate of the potential crack surface areas, better respecting the topology of the

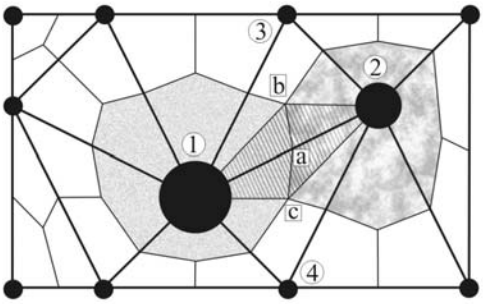

Figure 4. Example of two-dimensional tessellation of concrete mesostructure

random mesostructure, can in theory be obtained by using the dual complex (in the terminology of algebraic topology) of the Delaunay triangulation.

A straightforward dual is the well known Voronoi tessellation. However, for certain reasons (which for lack of space cannot be presented here), a modification of the Voronoi tessellation is needed (Cusatis 2003), as illustrated in Figure 4 for two dimensions. Consider the Delaunay triangles 123 and 124 which share the connecting strut 1-2 of the aggregates 1 and 2. The definition of the length of the contact line of the interacting aggregates (or area in three dimensions) may be obtained by connecting the points a, b and c in Figure 4. Point a is located at the middle way of the connection counterpart belonging to the matrix (l_m=l-R_1-R_2). Point b is the centre of mass of the area obtained by subtracting from the area of the 123-triangle the counterparts of the aggregate areas associated with that triangle; point c is similar to point b but related to the 124-triangle. Upon connecting points b and c to the aggregate centers, it is also possible to define more realistically the area (volume in three dimensions) associated to the connection 1-2 and represented by the dashed area in Figure 4.

This procedure can be applied to any of the connections emanating from a aggregate particle. In this way, one obtains a complete tessellation of the domain in which each cell contains one aggregate. The extension to the three-dimensional case is quite straightforward. The contact area of each connecting strut emanating from an aggregate is, in general, not planar and not orthogonal to the connection. For sake of simplicity, the constitutive law is imposed on the projection of this area on a plane orthogonal to the connection. The contact point, considered as the center of mass of the projected area, is no longer located along the connection. The eccentricity of this point requires small modifications in the definitions of the relative displacements at the contact point, and thus in the definitions of the strain components.

The formulation of the confinement effect has also been improved. The constitutive law is made to depend on the confinement strain transversal to the connection, instead of the confinement stress. In this way, the model becomes fully explicit (allowing explicit calculation of stresses from strains), and the numerical implementation more robust. The confinement strain, λ, in each connection is obtained by projecting orthogonally to the connection the average of the strain tensors of the adjacent tetrahedra. The strain tensor in each tetrahedron is computed assuming a linear distribution of displacements and neglecting the effect of particle rotations. The confinement effect is introduced by computing the initial post peak slope K_t of an assumed exponential softening for pure tensile behavior as follows (Cusatis 2003)

$$K_t = \frac{2E_N}{l_{cr}/l - 1} f(\lambda); \quad f(\lambda) = \frac{1}{1 + \langle -\lambda / \lambda_0 \rangle} \tag{5}$$

where l_{cr}=$2E_N G_t/\sigma_t^2$; E_N is the normal stiffness of the connection, σ_t is the tensile mesostrength. The characteristic strain parameter λ_0 governs the sensitivity to confining strain.

3.3 *Simulation of Unconfined Compressive Test*

Let us now examine the response sensitivity in the unconfined compressive test to the minimum aggregate size included in the lattice. The simulated specimens are prisms with a constant cross section of 75×75 mm^2 and height of 150 mm. Three series of six specimens are generated randomly, considering the following three granulometric distributions: 1) 5.4 % and 17.4 % (mass fractions) of aggregates with characteristic sizes of 16 mm and 12.5 mm, respectively; 2) 16.7 % and 8.4 % mass fractions of aggregates with sizes 9.5 mm and 8 mm are added to first series; 3) the combined granulometric distribution is further enhanced with 7 % and 4 % of aggregates with sizes 6.3 mm and 4.0 mm. The load is applied under displacement control considering loading platens with low friction (having the friction coefficient of 0.03).

The reference material properties are: cement content c=300 kg/m^3, water-cement ratio w/c=0.6, aggregate-cement ratio a/c=6.4. The assumed parameters of the constitutive law are the following: α=0.25, normal elastic modulus of cement E_c=11250 MPa, normal elastic modulus of aggregate E_a=6 E_c, tensile meso-strength (strength

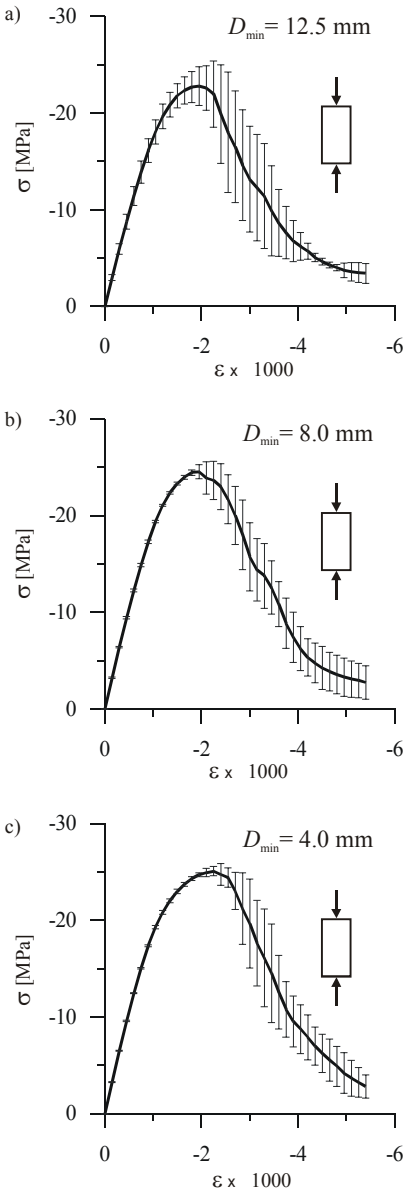

Figure 5. Stress-strain curves for a) D_{min}=12.5 mm, b) D_{min}=8.0 mm and c) D_{min}=4.0 mm.

at the meso-level of microstructure) σ_t=2.4 MPa; fracture energy at meso-level (without confining effect) G_t=0.03 N/mm; meso-cohesion $\sigma_s=3\sigma_t$, compressive meso-strength $\sigma_c=16\sigma_t$; hardening parameter at meso-level $K_c=0.26E_c$; shape parameter of compression cap β=1; asymptotic slope of the frictional hyperbola μ=0.2, $n_t=n_c$=2 (see Cusatis et al. 2003); and characteristic strain

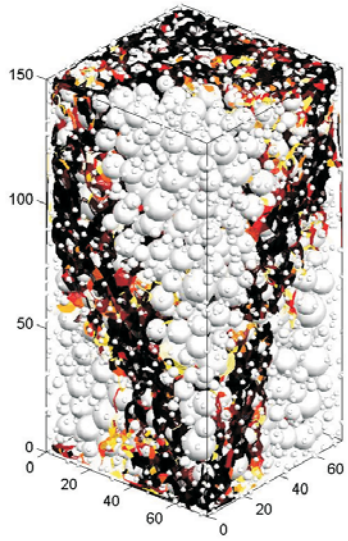

Figure 6. Damage localization at end of the test for a specimen with D_{min}=4.0 mm.

defining the confinement effect $\lambda_0=1\times10^{-3}$.

Figures 5a, b, c show the averaged nominal stress-strain curves of the three series of tests. The error bars represent the mean plus-minus standard deviation of six tests in each series. For the three series of tests the mean values of macroscopic Young's elastic modulus are 19,331 MPa, 21,376 MPa and 21,696 MPa, with the coefficients of variation 7.96%, 0.75% and 0.41%, respectively. The compressive strength values are obtained as 22.76 MPa, 24.50 MPa and 25.06 MPa with coefficient of variation equal to 6.52%, 2.49% and 1.76%, respectively, for the three test series. The results show that both macroscopic elastic modulus and compressive strength tend to converge to a certain fixed value as the simulation of the entire granulometric curve, from the largest aggregate size to the smallest one, is improved. Also, the coefficient of variation tends to decrease, confirming the isotropic character of the macroscopic concrete behavior up to the peak (before any damage localization). It may thus be concluded that the model can indeed realistically simulate the mesolevel interaction between the aggregates and the cement paste. The minimum aggregate sizes introduced into the simulation may be considered as a parameter which governs the accuracy of the simulations; they play a similar role as the characteristic finite element size in a finite element mesh.

Let us now examine the postpeak response. In the softening branch of the stress-strain curve, the damage localizes, as seen clearly in Figure 6 for one of the specimens of the third series (minimum aggregate size 4.0 mm) at the end of the test. Because of localization, the macroscopic response is no longer isotropic, and this explains why the standard deviation increases significantly in the postpeak. Note also that, in the softening regime, the reduction of the standard deviation due to the minimum aggregate size introduced into the analysis is not as pronounced as for the behavior up to the peak. The explanation is that damage localization is mostly influenced by the maximum aggregate size which is the same in all series of tests.

4 ACKNOWLEDGMENT

The work of Bažant and Caner was partially supported under the U.S. National Science Foundation grant CMS-9732791 to Northwestern University. M. Polli and G. Merlo of Politecnico are thanked for help in M4 and lattice simulations.

5 REFERENCES

Batdorf, S.B. & Budianski, B. 1949. *A mathematical theory of plasticity based on the concept of slip*. Technical Note No. 1871. Nat. Advisory Committee for Aeronautics, Washington, D.C.

Bažant, Z. P. 1984. Imbricate continuum and its variational derivation. *Journal of Structural Engineering, ASCE*, 110, pp.1693-1712.

Bažant, Z.P. & Caner, F. 2002. *Microplane model M5 with kinematic and static constraints for concrete fracture and anelasticity*. Structural Engineering Report No. 02-12/C699m, Northwestern University, Evanston, Illinois; also *J. of Engrg. Mech. ASCE*, submitted to.

Bažant, Z. P., Caner, F., Carol, I., Adley, M. & Akers, S.A. 2000. Microplane Model M4 for Concrete. I: formulation with work-conjugate deviatoric stress. *Journal of Engineering Mechanics, ASCE* 126, No. 9, pp. 944-953.

Bažant, Z. P. & Di Luzio, G. 2003. Nonlocal microplane model with strain-softening yield limits. *Int. J. of Solids and Structures*. in press.

Bažant, Z.P. & Prat, P. 1988. Microplane model for brittle plastic materials: I. Theory. *Journal of Engineering Mechanics, ASCE,* 114, No. 10, pp. 1672-1688.

Bažant, Z. P. & Ožbolt, J. 1990. Nonlocal microplane model for fracture, damage and size effect in structures. *Journal of Engineering Mechanics, ASCE,* 116, No. 11, pp. 2485-2505.

Bažant, Z.P., Xiang, Y. & Prat, P.C. 1996. Microplane model for concrete. I. Stress-strain boundaries and finite strain. *Journal of Engineering Mechanics, ASCE*, 122, No. 3, pp. 245-254.

Brocca, M. & Bažant, Z.P. (2000). Microplane constitutive model and metal plasticity. *Applied Mechanics Reviews, ASME* 53 (10), 265--281.

Bronkhorst, C.A., Kalindindi, S.R. & Anand, L. 1992. Polycrystalline plasticity and the evolution of crystallographic texture. in fcc metals. *Phil. Trans. R. Soc. London*, A341, 443-477.

Butler, G.C. & McDowell, D.L. 1998. Polycrystal constraint and grain subdivision. *International Journal of Plasticity* 14 (8), pp. 703-717.

Camacho, G.T. & Ortiz, M. 1996. Computational modeling of impact damage in brittle materials. *International Journal of Solids and Structures,* 33 (20-22), 2899-2938.

Caner, F.C. & Bažant, Z.P. 2000. Microplane model M4 for concrete: II. Algorithm and Calibration. *Journal of Engineering. Mechanics ASCE,* 126 (9), 954--961.

Cusatis G. 2003. *Private communication to Z.P. Bažant*. Sept. 22.

Cusatis G., Bažant Z.P. & Cedolin L. 2003a. Confinement-shear lattice model for concrete damage in tension and compression: I. Theory." *Journal of Engineering Mechanics, ASCE,* 129(12), in press.

Cusatis G., Bažant Z.P. & Cedolin L. 2003b. Confinement-shear lattice model for concrete damage in tension and compression: II: Numerical implementation and Validation. *Journal of Engineering Mechanics, ASCE* 129(12), in press.

Di Luzio, G. 2002. *A new nonlocal microplane model for fracture and damage of concrete*. PhD Thesis. Department of Structural Engineering, Politecnico di Milano.

Di Luzio, G., Cedolin, L. & Merlo, G. 2003. *A symmetric over-nonlocal microplane model M4 for concrete*. Report (November 2003). Dipartimento di Ingegneria Strutturale, Politecnico di Milano.

Hillerborg, A., Modéer, M. & Petersson, P.E. 1976. Analysis of crack formation and crack growth in concrete by means of fracture mechanics and finite elements. *Cement and Concrete Research,* 6, 773--782.

Taylor, G.I. 1938. Plastic strain in metals. *J. Inst. Metals,* 62, 307--324.